



Totally volume integral of fluxes for discontinuous Galerkin method-two dimensional Euler equations.

Elhadi I. Elhadi ^a, Abdelhadi A. Buzghaiba ^{b,*}, Mouad A. Fakroon ^b

^aDepartment of mechanical engineering, Faculty of Engineering, University of Benghazi, Benghazi, Libya

^bDepartment of Aeronautical Engineering, Faculty of Aeronautical Sciences, University of Bright Star, Berega, Libya.

Highlights

- The totally volume discontinuous Galerkin (TVI-DG) works efficiently for the problems, whether shock appears or not.
- The Riemann problem with different types of waves has been accurately solved.
- As the time of getting, the solution by the present method is plainly short.

ARTICLE INFO

Article history:

Received 28 February 2021

Revised 14 June 2021

Accepted 28 August 2021

Keywords:

Euler equations, discontinuous Galerkin method, Divergence theorem, Riemann problems.

*Address of correspondence:

E-mail address: Abdelhad.buzghaiba@gmail.com.

A. A. Buzghaziba

ABSTRACT

In this paper, the scheme of constructing high-order accurate totally volume discontinuous finite element method for the numerical solution of the 1D Euler equations is extended to 2D Euler equations on Cartesian meshes. In the present work, the boundary integral fluxes are transformed into volume integral by applying divergence theorem to the boundary integral of the Riemann fluxes. Therefore, the totally volume discontinuous finite element is independent on the boundary integral fluxes at the element boundaries as opposed to the classical discontinuous Galerkin method. The accuracy is obtained by applying high-order polynomial approximations within elements using the tensor product of Lagrange polynomial. For temporal integration, strong stability preserving Runge-Kutta method SSPRK (3, 3) is applied. The scheme is stabilized by using Streamline Upwind Petrov Galerkin (SUPG) stabilization technique. For the spatial discretization, the polynomial of order 1 and 2 are used, the shape function is constructed for the master (computational) element after applying the coordinate transformation for the physical domain, the transformation for the governing equations is performed to get it in the function of computational Cartesian, then the governing equations are put in conservative form. The numerical results of applying totally volume integral discontinuous Galerkin method for two-dimensional Euler equations presented in this paper show that the scheme is very accurate, fast, and effective even with shock appearance.

1. Introduction

The original discontinuous Galerkin method (DG) was introduced by (Reed and Hill, 1973) for solving the neutron transport (linear hyperbolic equations). There are several methods that use DG formulation to discretize the governing equations. A major development of the DG method was realized by Cockburn and Shu, 1989; Cockburn and Shu, 1990; Cockburn and Shu, 1998; Cockburn, 1991 and Cockburn *et al.* 2009), these papers introduced and developed the well-known Runge-Kutta discontinuous Galerkin (RKDG) method and the local discontinuous Galerkin (LDG), which is an extension of RKDG for solving the convection-diffusion problems like the Navier-Stokes equations. In general, the LDG method treats the solutions of the second or higher spatial derivatives. The basic idea of LDG is to rewrite the original equations as large systems of first-order differential equations and then discretize them by using RKDG method. In this work, we extend the previous work of constructing high order accurate totally volume discontinuous Galerkin for the numerical solution of the 1D Euler equations (Elhadi and Rustum, 2017) to 2D Euler equations on Cartesian meshes.

2. Totally volume discontinuous Galerkin formulation

2.1. Space discretization

For the numerical solution of Euler equations by using TVI-DG the Euler equations can be written in a conservative form as in classical DG. Euler equations in the conservative form are written as

$$\frac{\partial Q}{\partial t} + \nabla \cdot F(Q) = 0 \quad (1)$$

With fitted initial-boundary conditions. Where Q is a vector of conservative variables and $F(Q)$ is a vector of fluxes in two dimensions with its Cartesian components $f(Q)$ and $g(Q)$. The conservative variables Q and the Cartesian components $f(Q)$ and $g(Q)$ of the flux $F(Q)$ are expressed as:

$$Q = \begin{bmatrix} \rho \\ \rho u \\ \rho v \\ \rho e \end{bmatrix}, f(Q) = \begin{bmatrix} \rho \\ \rho u^2 + p \\ \rho uv \\ \rho hu \end{bmatrix}, g(Q) = \begin{bmatrix} \rho v \\ \rho uv \\ \rho v^2 + p \\ \rho hv \end{bmatrix} \quad (2)$$

where ρ is the fluid density u and v are the velocity components, p is the pressure, e is the total internal energy per unit mass, and the total enthalpy per unit mass h can be defined as $h = e + p/\rho$. By assuming that the fluid is a perfect gas, then p can be estimated as $p = (\gamma - 1)\rho(e - u^2/2)$, where γ is the specific heat ratio of the fluid. By multiplying by a "weight function" w , integrating over the domain Ω , and performing integration by parts we get the weak form of the problem:

$$\int_{\Omega} w \frac{\partial Q}{\partial t} d\Omega + \oint_{\Gamma} w F(Q) \cdot n d\Gamma - \int_{\Omega} \nabla w \cdot F(Q) d\Omega = 0 \quad (3)$$

where Γ indicates the boundary of element E and Ω is the volume of the element. By subdividing the domain Ω into non-overlapping elements E , $\Omega = \cup_{j=1}^N \Omega_h$ and by assuming functions Q_h and w_h ,

defined within each element, given as the linear combination of n shape functions Φ_i

$$Q_h(X, t) = \sum_{i=1}^n Q_i(t)\Phi_i(X) \tag{4}$$

$$w_h(X) = \sum_{i=1}^n w_i\Phi_i(X) \tag{5}$$

The coefficients Q_i and w_i indicate the degrees of freedom of the numerical solution of the state variable and the test function for every element E . Eq. (3) is valid to each element Ω_h , applying Eq. (3) to each element over the entire domain yields:

$$\int_{\Omega_h} [w_h \frac{\partial Q_h}{\partial t} - \nabla w_h \cdot F(Q_h)] d\Omega_h + \int_{\Gamma_h} w_h F(Q_h) \cdot \mathbf{n} d\Gamma_h = 0 \tag{6}$$

where Γ_h denotes the boundary of the element E and \mathbf{n} is an outward vector normal to the boundary. Since the weight function consists of a linear combination of shape n functions, Eq. (6) is valid for each shape function in the weight function, by replacing the weight function with any of its shape functions yields to

$$\int_{\Omega_h} [\Phi_i \frac{\partial Q_h}{\partial t} - \nabla \Phi_i \cdot F(Q_h)] d\Omega_h + \int_{\Gamma_h} \Phi_i F(Q_h) \cdot \mathbf{n} d\Gamma_h = 0 \tag{7}$$

a system of n equations is constructed. The flux that appeared at the last term can be replaced by the numerical flux due to discontinuity at the interface between the elements, so the $F(Q_h) \cdot \mathbf{n}$ is replaced by numerical flux function $F_u(Q_h^-, Q_h^+)$ which depends on the internal interface state Q_h^- , and on the neighboring element interface state Q_h^+ , and on the direction \mathbf{n} normal to the interface in this work the Lax flux (LF) is applied at the boundaries with the following formulation:

$$f_u(Q^+, Q^-) = 0.5[f(Q^+) + f(Q^-) - \alpha(Q^+ - Q^-)] \tag{8}$$

where α is an estimate of the biggest eigenvalue of the Jacobian matrix (Toro, 1999).

In order to unify the integrals (surface integral and volume integral), the totally volume integral of the upwind flux scheme for DG method is used for this purpose. This can be achieved by using the relation between surface and volume integrals for any vector B , which is given by the divergence theorem as:

$$\oint_{\Gamma} B \cdot \mathbf{n} d\Gamma = \iiint_V \nabla \cdot B dV \tag{9}$$

where Γ and V are the surface and volume of the problem domain.

The totally volume integral DG method is obtained by applying the divergence theorem to the last term of Eq. (7) and rearrangement to give the following form

$$\int_{\Omega_h} [\Phi_i \frac{\partial Q_h}{\partial t} - \nabla \Phi_i \cdot F(Q_h) + \nabla(\Phi_i F_u(Q_h))] d\Omega_h = 0 \tag{10}$$

where $F(Q_h)$ is the physical flux and $F_u(Q_h)$ is numerical flux, both physical and numerical flux can be approximated by a polynomial of order n as done for the Q_h and w_h

$$F(Q_h) = \sum_{i=1}^n F_i(Q_h)\Phi_i, F_u = \sum_{i=1}^n F_{u,i}\Phi_i \tag{11}$$

For two dimensions the Eq. (10) can be written as

$$\int_{\Omega_h} [\Phi_i \frac{\partial Q_h}{\partial t} - \frac{\partial \Phi_i}{\partial x} f(Q_h) + \Phi_i \frac{\partial f_u(Q_h)}{\partial x} + \frac{\partial \Phi_i}{\partial x} f_u(Q_h) - \frac{\partial \Phi_i}{\partial y} g(Q_h) + \Phi_i \frac{\partial g_u(Q_h)}{\partial y} + \frac{\partial \Phi_i}{\partial y} g_u(Q_h)] dx dy = 0 \tag{12}$$

By assembling all the elemental contributions, the system of ordinary differential equations which govern the evolution in time of the discrete solution can be written as:

$$M \frac{dQ}{dt} = R(Q) \tag{13}$$

$$\frac{dQ}{dt} = L \tag{14}$$

where,

$$L(Q) = M^{-1}R(Q) \tag{15}$$

where M denotes the mass matrix, Q is the global vector of the number of degrees of freedom, and $R(Q)$ is the residual vector. In order to describe the geometry of the elements and define the shape functions employed in this work, 2D Quadrilateral Elements are employed in the present work. The shape functions are written by using Lagrangian functions for normalizing elements after applying coordinate transformation in order of getting the master element.

2.2. Temporal discretization

In the present work high order Runge-Kutta method SSPRK(3,3) is used to approximate the solution of the ODE (semi-discrete equation) of the form:

$$\frac{dQ}{dt} = L(Q) \tag{16}$$

The RK (3,3) can be expressed in the following form:

$$Q^{(1)} = Q^{(m)} + \Delta t L(Q^{(m)}) \tag{17a}$$

$$Q^{(2)} = \frac{3}{4}Q^{(m)} + \frac{1}{4}[Q^{(1)} + L(Q^{(1)})] \tag{17b}$$

$$Q^{(m+1)} = \frac{1}{3}Q^{(m)} + \frac{2}{3}[Q^{(2)} + L(Q^{(2)})] \tag{17c}$$

where $Q^{(m)}$ is the solution at a time t_m and $Q^{(m+1)}$ is the solution at the next step of time after the intermediate m steps are applied. The formulation of Courant number (CFL) used in this work can be written as:

$$CFL = \Delta t \sum_{i=1}^{i=d} \frac{\lambda_i}{\Delta x_i} \tag{18}$$

where d is the number of coordinates dimension, λ is the absolute maximum eigenvalue of the Jacobian matrix and Δx is the maximum length of the element, Δt is the time step size.

2.4. The Stabilization technique

The main idea is to use the Taylor series expansion of the weighting functions along with the streamline directions. Thus, in the streamline upwind, the weighting function is perturbed by the term acting along with the characteristic directions. This is realized by additional term to the weighting function (test function) Thus for the weighting function as defined in Eq. (5) with the perturbation can be written as in Nowakowski et al. (2011):

$$w_h(X) = \sum_{i=1}^n [\Phi_i(X) + \beta \Delta t \lambda \cdot \nabla \Phi_i(X)] \tag{19}$$

where λ is the absolute maximum eigenvalue of the governing equation Δt is the time step. Substituting into Eq. (10) for two dimensions by assembling all the elemental contributions the system of ordinary differential equations, which govern the evolution in time of the discrete solution, can be obtained :

$$\int_{\Omega_h} [\Phi_i \frac{\partial Q_h}{\partial t} - \frac{\partial \Phi_i}{\partial x} f(Q_h) + \Phi_i \frac{\partial f_u(Q_h)}{\partial x} + \frac{\partial \Phi_i}{\partial x} f_u(Q_h) - \frac{\partial \Phi_i}{\partial y} g(Q_h) + \Phi_i \frac{\partial g_u(Q_h)}{\partial y} + \frac{\partial \Phi_i}{\partial y} g_u(Q_h) + \beta \Delta t \lambda_x^2 \frac{\partial \Phi_i}{\partial x} \frac{\partial Q_h}{\partial x} + \beta \Delta t \lambda_y^2 \frac{\partial \Phi_i}{\partial y} \frac{\partial Q_h}{\partial y}] dx dy = 0 \tag{20}$$

The last equation has the stabilization parameters $\beta\Delta t\lambda_x^2$ and $\beta\Delta t\lambda_y^2$ which means the solution is stable with suitable stabilization parameters, where λ_x and λ_y are the maximum eigenvalues in x and y directions, respectively Nowakowski et al. (2011).

2.3. The Numerical results

Three numerical problems are selected to test the performance of the numerical scheme; the tests are also used to illustrate some typical wave patterns resulting from the solution of the problems, which are the Riemann problems. In order to test the effectiveness of the scheme, three different behavior of problems is considered: problem with the exact solution, problem with initial discontinuity (Riemann problem), and the problem with shock formation. Both the initial data and the results shown in the following figures are in terms of primitive variables. In all cases, the ratio of specific heat is 1.4.

2.3.1. Test example 1

The first example is the two dimensional Euler equations proposed in (Jiang and Shu, 1996) with initial conditions presented as:

$$(\rho, u, v, p) = (1. + 2 \sin(\pi(x + y)), 0.7, 0.3, 1.)$$

The exact solution is given as $\rho(x, y, t) = 1. + 2 \sin(\pi((x + y) - (u + v)t))$, with $u = 0.7, v = 0.3$. The domain of the problem is $[0,4] \times [0,4]$. The domain is divided into equal elements, $\Delta x = \Delta y = 1/10, 1/20, 1/40, 1/80$ and $1/160$. Table 1 shows the time steps with corresponding size steps for different orders of polynomials. The TVI-DG are applied with a polynomial of order 1 and 2. The numerical results are calculated at time equals 2.

Table 1

Time steps with corresponding size steps for a different order of polynomials

	$k=1$	$k=2$
$\Delta x = \Delta y$	Δt	Δt
1/20	1/50	1/100
1/40	1/100	1/200
1/80	1/200	1/400
1/160	1/400	1/800

Table 2 shows the L_1, L_∞ norms and the order of accuracy when $k = 1$ and RK (3, 3) are performed at $t=2$, the flux used at the boundaries is LF, the data contained in the table displays the effectiveness and the accuracy of the method. The table uses two significant indicators to show the effectiveness of the scheme, error and the order of accuracy; it is observed that the order of accuracy is greater than the order of the polynomial by about 1.53, which means that the rate of convergence of the scheme is acceptable.

Table 2

The errors L_1, L_∞ and order of accuracy for 2D Euler equations with periodic boundary conditions at $t = 2$ by using a polynomial of order $k=1$, with Lax flux

$N(\text{number of elements})$	L_1	Order	L_∞	Order
100	1.90e-2		3.53e-2	
400	2.22e-3	3.10	5.82e-3	2.60
1600	4.15e-4	2.42	1.21e-3	2.26
6400	9.80e-5	2.08	2.76e-4	2.13

Table 3 shows that the L_1, L_∞ norms and the order of accuracy when $k = 2$ and RK (3, 3) are applied at $t=2$, the flux used at the boundaries is LF, The data achieved in the table shows that the scheme works effectively. The order of accuracy is greater than the order of the polynomial, which means that the rate of convergence of the scheme is satisfactory.

Table 3

The errors L_1, L_∞ and order of accuracy for 2D Euler equations with periodic boundary conditions at $t = 2$ by using a polynomial of order $k = 2$

$N(\text{number of elements})$	L_1	Order	L_∞	Order
100	5.91e-3		1.19e-2	
400	1.09e-3	2.44	2.19e-3	2.44
1600	1.97e-4	2.47	3.97e-4	2.46
6400	2.92e-5	2.75	5.8e-5	2.78

Table 4 shows the computational time of the present TVI-DG method in comparison with the computational time that was achieved in Elhadi (2011). The current CPU time is obtained using (Intel(R) Core(TM) i5-4200M CPU@ 2.5 GHz (4 CPUs) 4096 RAM). It can be seen that the present method CPU time is extremely quick in comparison with NDG method. These results are obtained when $k = 2$ and RK (3,3) are applied at $t = 2$, the flux used at the boundaries is LF.

Table 4

The CPU time in seconds for the 2D Euler equations with the periodic boundary conditions at $t = 2$ using the polynomial of order $k = 2$

$N(\text{number of elements})$	$CPU(S), NDG$	$CPU(S), TVI-DG$
100	4.65	0.6
400	37.88	4.55
1600	303.44	36.28
6400	2507.02	292.13

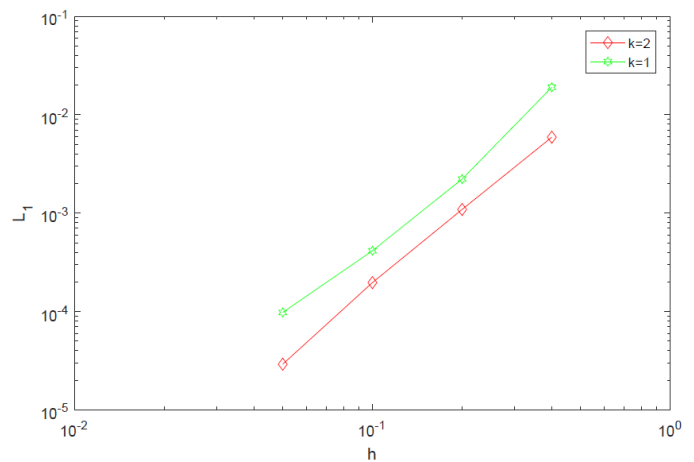


Fig. 1. Comparison of L_1 errors of the $k=1$, and 2 for test 4 at $t=2$, with LF, for 100, 400, 1600, and 6400 elements

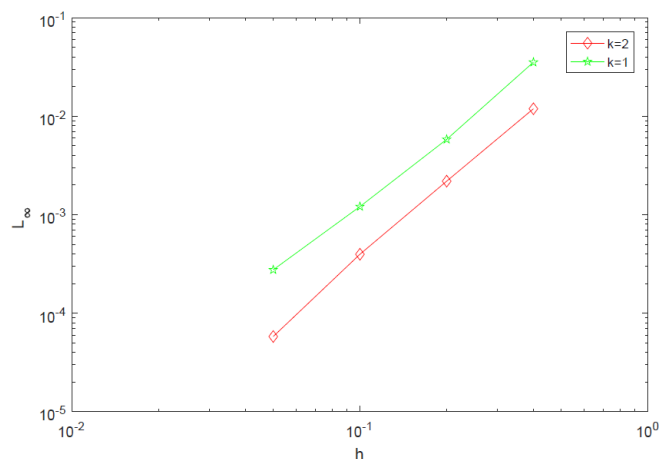


Fig. 2. Comparison of L_∞ errors of the $k=1$ and 2 for test 4 at $t=2$, with LF, for 100, 400, 1600, and 6400 elements

Fig. 1 and Fig. 2 show the errors of L_1 and L_∞ for the test problem at different mesh sizes with $k=1$ and $k=2$, the figures reveal that

all errors decrease whether with increasing of the order of polynomials or with decreasing of mesh size, these results indicate the effectiveness of the TVI-DG method.

2.3.2. Test example 2

The second test example is a Mach 3 wind tunnel step (forward-facing step problem) in two dimension flow cases. It was initially proposed in (Woodward and Colella, 1984). The present computational results are obtained by using N equally elements of the size $\Delta x = \Delta y = 1/160$ with corresponding time step $\Delta t=1/12800$. The boundary conditions applied are the supersonic inflow from the left and the supersonic outflow to the right, while the slip boundary conditions (reflecting boundary conditions) are performed for the upper and lower and the face at the forward step. The initial data is presented as $(\rho, u, v, p) = (1.4, 3, 0, 1.)$ The numerical boundary flux is performed by using the LF. The time discretization is applied by using RK (3, 3) for the TVI-DG of the polynomials of orders $k = 1$.

2.3.2. Test example 2

The second test example is a Mach 3 wind tunnel step (forward-facing step problem) in two dimension flow cases. It was initially proposed in (Woodward and Colella, 1984). The present computational results are obtained by using N equally elements of the size $\Delta x = \Delta y = 1/160$ with corresponding time step $\Delta t=1/12800$. The boundary conditions applied are the supersonic inflow from the left and the supersonic outflow to the right, while the slip boundary conditions (reflecting boundary conditions) are performed for the upper and lower and the face at the forward step. The initial data is presented as $(\rho, u, v, p) = (1.4, 3, 0, 1.)$ The numerical boundary flux is performed by using the LF. The time discretization is applied by using RK (3, 3) for the TVI-DG of the polynomials of orders $k = 1$.

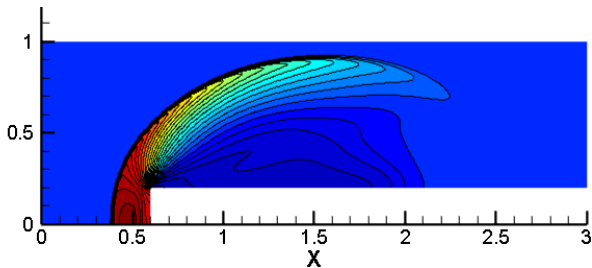


Fig. 3. The density contours for the forward facing step problem, $\Delta x = \Delta y = 1/160, k=1, t = 0.5$

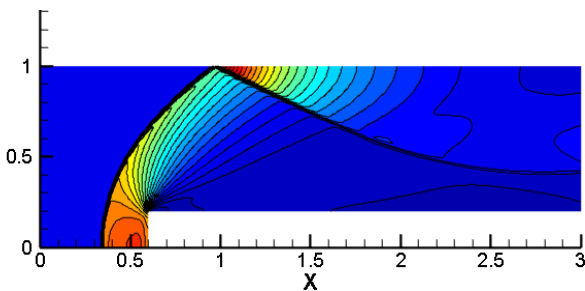


Fig. 4. The density contours for the forward facing step problem, $\Delta x = \Delta y = 1/160, k=1, t = 1$

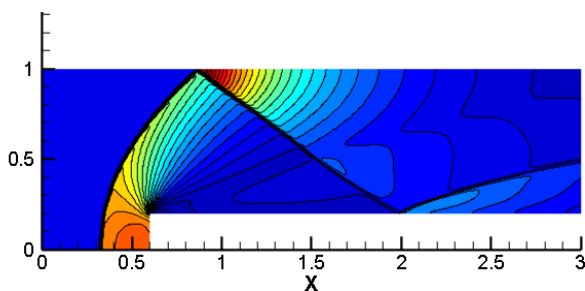


Fig. 5. The density contours for the forward facing step problem, $\Delta x = \Delta y = 1/160, k=1, t = 1.5$

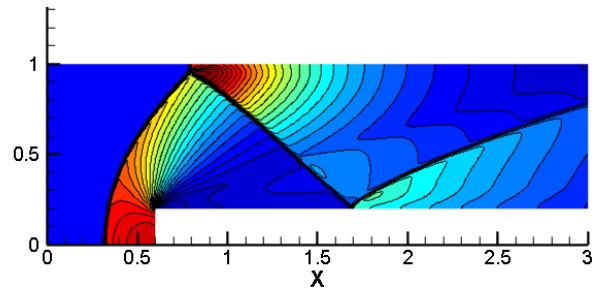


Fig. 6. The density contours for the forward facing step problem, $\Delta x = \Delta y = 1/160, k=1, t = 2$

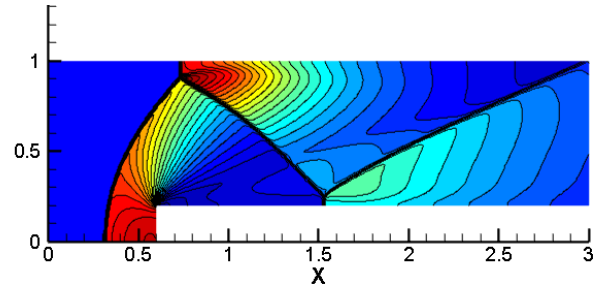


Fig. 7. The density contours for the forward facing step problem, $\Delta x = \Delta y = 1/160, k=1, t = 2.5$

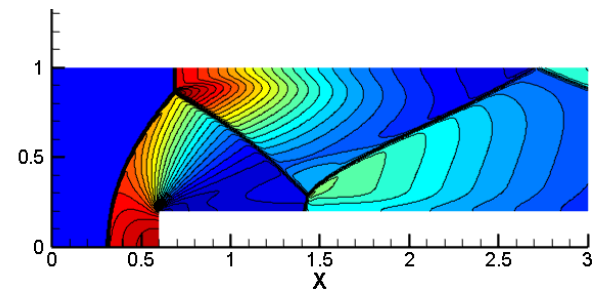


Fig. 8. The density contours for the forward facing step problem, $\Delta x = \Delta y = 1/160, k=1, t = 3$

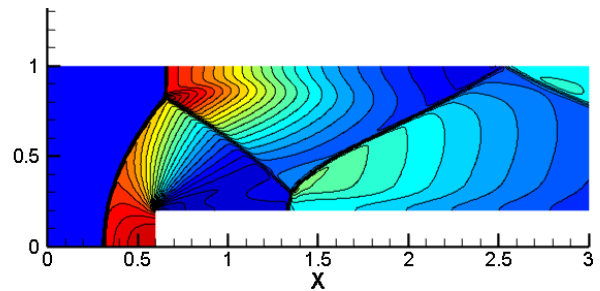


Fig. 9. The density contours for the forward facing step problem, $\Delta x = \Delta y = 1/160, k=1, t = 3.5$

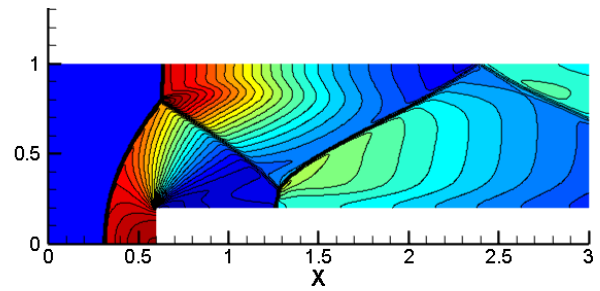


Fig. 10. The density contours for the forward facing step problem, $\Delta x = \Delta y = 1/160, k=1, t = 4$

Figures from Fig. 3 to Fig. 10 show the density contours (30,0.2365-5.647), (30,0.268-7.564), (30,0.2805-7.717), (30,0.2668-6.65), (30,0.2668-6.602), (30,0.2673-6.383), (30,0.27-

6.5) and (30,0.275-6.1) for the forward-facing step problem by using TVI-DG at $t=0.5, 1, 1.5, 2, 2.5, 3, 3.5$ and 4 by using polynomial of order $k=1$ with mesh size of $\Delta x = \Delta y = 1/160$, LF flux is applied at the boundaries. The figures display the behavior of the solution at different times, the figures reveal the gradualism of formation, reflections, and the interactions of shock lines at the lower, facing, and the upper walls.

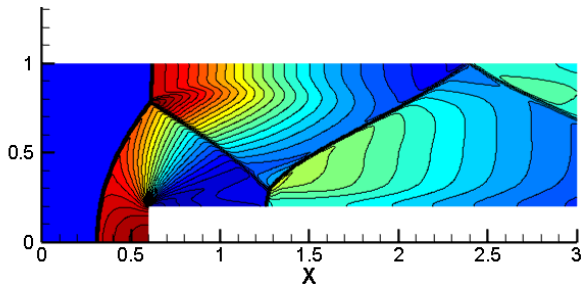


Fig. 11. The density contours for the forward facing problem, $\Delta x = \Delta y = 1/160, k = 2, \beta = 2.5, t = 4$

Fig. 11 displays the density contour (30, 0.25-6.1) for the forward-facing step problem by using TVI-DG at $t = 4, k = 2$ with a mesh size of $\Delta x = \Delta y = 1/160$, LF flux is applied at the boundaries. The main observation is that the shock width is thinner than in Fig. 10. In addition, the second reflection of shock waves on the upper wall occurs at a position about $x = 2.4$.

2.3.3. Test example 3

The third example is considered as two dimensional Riemann problem which is introduced in Brio et al. (2011). Initial data can be written as:

$$\text{If } 1 \leq x \leq 2 \text{ and } 1 \leq y \leq 2 \quad (\rho, u, v, p) = (0.5312, 0, 0, 0.4)$$

$$\text{If } 0 \leq x \leq 1 \text{ and } 1 \leq y \leq 2 \quad (\rho, u, v, p) = (1, 0.7276, 0, 1)$$

$$\text{If } 0 \leq x \leq 1 \text{ and } 1 \leq y < 2 \quad (\rho, u, v, p) = (0.8, 0, 0, 1)$$

$$\text{If } 1 \leq x \leq 2 \text{ and } 0 \leq y < 1 \quad (\rho, u, v, p) = (1, 0, 0.7276, 1)$$

The proposed problem consists initially of two contact discontinuities and two shock waves, one of the contact discontinuities occurs between the third and second quadrants and the other exists between the third and fourth quadrants. Density contours at $t=0$ (initial) are displayed in Fig. 12 TVI-DG is applied with the order of polynomial $k=1$, with mesh size $\Delta x = \Delta y = 1/400$ with corresponding Time step $\Delta t = 1/4000$. RK (3,3) is used for temporal discretization, the numerical flux at boundaries performed is LF. The results are obtained at the time, $t=0.52$.

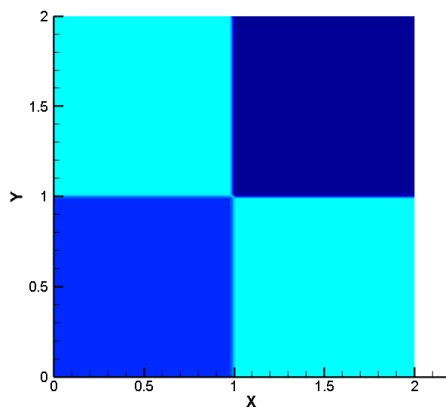


Fig. 12. The density contours 29 $\rho:(0.53-1.71)$ for test example 3 at $t=0$

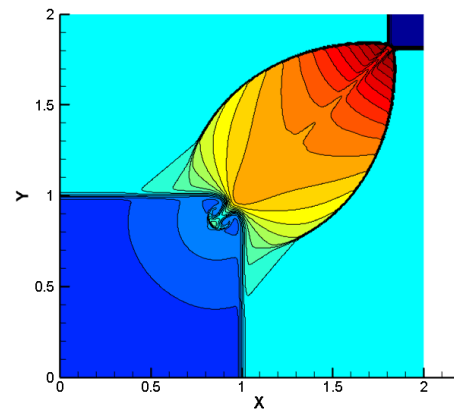


Fig. 13. The density contours 30 $\rho:(0.53 - 1.71)$ obtained using RK-TVI, $\Delta x = \Delta y = 1/400$, RK (3, 3), LF, $t=0.52$

Fig. 13 shows the pattern of the solution, the main observation is that the interaction of two shocks that is occurred between the second and first quadrants and the shock that is existed between the first and fourth quadrants. In addition, the contact lines encounter the sonic circle of constant state in the third quadrant and bend to the end in spirals inside the subsonic area of the circle's portion lying in this quadrant. Due to interaction between the Mach shocks the three pairs of shocks have appeared so, the subsonic zone is surrounded by two joining Mach shocks and the reflected shocks. The last observation is that the shocks that appeared are thin reflecting the strength of the scheme.

3. Conclusions

Constructing high-order accurate totally volume discontinuous finite element method for the numerical solution of the 2D Euler equations as an extension of 1D Euler equations on cartesian meshes has been made successfully. The boundary integral fluxes are transformed into volume integral by applying divergence theorem to the boundary integral of the Riemann fluxes. The numerical results are obtained by applying totally volume integral discontinuous Galerkin method for different problems that involve smooth solution, initial discontinuity (Riemann problem), and shock formation. Based on the results of the present study, the following observations and inferences can be drawn:

1. The totally volume discontinuous Galerkin (TVI-DG) works very efficiently for the considered test problems, whether shock appears or not. Furthermore, the analysis of the results for the Riemann problems in 2D, which is consisted of different types of discontinuities like shock waves and contact also their reflections and interactions show that the scheme plainly describes the behavior of the solution with all its details.
2. The stabilization parameter β depends on the type of intensity of the discontinuity, the mesh size, and the time step used. The main observation is that the stabilization parameter β has to be minimum, because its main function is to capture the oscillations, and if the stabilization factor β is larger than the required value to keep the solution smooth, the solution will be less accurate.
3. As for the speed of getting the solution, the TVI-DG is faster than NDG by about nine times which is considered a satisfactory result, this acceleration is a result of the disappearance of boundary integral over the cell and transfers it to the integral over the volume which makes the implementation of the code more suitable to get the fast and accurate solution.

References

Brio, M., Zakharian, A.R. and Webb, G.M. (2001) 'Two-dimensional Riemann solver for Euler equations of gas dynamics', *Journal of Computational Physics*, 167(1), pp. 177–195.

- Cockburn, B. & Shu, C. W. (1998) 'The Runge-Kutta discontinuous Galerkin methods for conservation laws V: Multidimensional systems', *Journal of Computational Physics*, 141, pp. 199-224.
- Cockburn, B. (1991) 'The Runge kutta local projection p1-discontinuous Galerkin finite element method for scalar conservative laws', *Mathematical Modelling and Numerical Analysis*, 25, pp. 337-361.
- Cockburn, B. & Shu, C. W. (1989) 'TVB Runge-Kutta local projection discontinuous Galerkin finite element method for conservation laws II: General framework', *Mathematics of Computation*, 52, pp. 441-435.
- Cockburn, B., Hou, S. & Shu, C.-W. (1990) 'The Runge-Kutta local projection discontinuous Galerkin finite element method for conservation laws. IV: The multidimensional case', *Mathematics of Computation*, 54, pp. 545-581.
- Cockburn, B., and & Shu, C. W. (1990) 'The Runge-Kutta local projection discontinuous Galerkin finite element method for conservative laws: The multidimensional case', *Journal of Computational Physics*, 54, p. 39.
- Elhadi, E.I and Rustum, I.M. (2017) 'Totally Volume Integral of Fluxes for Discontinuous Galerkin Method (TVI-DG) II-One Dimensional System of Equations', *Libyan Journal for Engineering Research*, 1, 2, pp. 60-64
- Elhadi, E.I. (2011) 'Modified Streamline Upwind Petrov-Galerkin Method'. (Doctoral Dissertation), University of Sheffield.
- Jiang, G.S. and Shu, C. W. (1996) 'Efficient implementation of weighted ENO schemes', *Journal of Computational Physics*, 126(1), pp. 202 – 228.
- Nowakowski, A. F. Elhadi, E. I. and Qin, N. (2011) 'Modified streamline Petrov formulation for discontinuous Galerkin method', In: *16th International Conference on Finite Elements for Flow Problem*, FEF2011, Munich, Germany, 23-25 March.
- Reed, W. R. & Hill, T. R. (1973) 'Triangular mesh methods for the neutron transport equations', *Los Alamos Scientific laboratory report, LA-UR-73-479*, 72.
- Toro, E. F.(1999) '*Riemann solvers and numerical methods for fluid dynamics*', Second edn, (Springer).
- Woodward, P. & Colella, P. (1984) 'The numerical simulation of two-dimensional fluid flow with strong shocks', *Journal of Computational Physics*, 54, pp. 115-173.